Title

Coexistence of Multilayered Phases of Confined Water: The Importance of Flexible Confining Surfaces



Journal

ACS Nano, 12(1)

ISSN

1936-0851

Authors

Pestana, Luis Ruiz

Felberg, Lisa E

Head-Gordon, Teresa

Publication Date

2018-01-23

DOI

10.1021/acsnano.7b06805

Peer reviewed

# Coexistence of Multilayered Phases of Confined Water: The Importance of Flexible Confining Surfaces

Luis Ruiz Pestana[1], Lisa E. Felberg[2], Teresa Head-Gordon[1-5*]

[1]Chemical Sciences Division, Lawrence Berkeley National Laboratory
[2]Department of Chemical and Biomolecular Engineering, [3]Department of Chemistry,
[4]Department of Bioengineering, [5]Pitzer Center for Theoretical Chemistry
University of California, Berkeley
Berkeley, CA 94720

**Abstract**

Flexible nanoscale confinement is critical to understanding the role that bending fluctuations play on biological processes where soft interfaces are ubiquitous, or to exploit confinement effects in engineered systems where inherently flexible 2D materials are pervasively employed. Here, using molecular dynamics simulations, we compare the phase behavior of water confined between flexible and rigid graphene sheets as a function of the in-plane density, $\rho_{2D}$. We find that both cases show commensurate mono-, bi-, and tri-layered states, however the water phase in those states and the transitions between them are qualitatively different for the rigid and flexible cases. The rigid systems exhibit discontinuous transitions between an (n)-layer and an (n+1)-layer state at particular values of $\rho_{2D}$, whereas under flexible confinement the graphene sheets bend to accommodate an (n)-layer and an (n+1)-layer state coexisting in equilibrium at the same density. We show that the flexible walls introduce a very different sequence of ice phases and their phase co-existence with vapor and liquid phases than that observed with rigid walls. We discuss the applicability of these results to real experimental systems to shed light on the role of flexible confinement and its interplay with commensurability effects.

Keywords: nanoconfinement, graphene, phase coexistence, commensurability effects, 2D materials

*corresponding author: thg@berkeley.edu

The phase behavior and properties of water under nanoconfinement are significantly different than in the bulk, which has important implications for a myriad of nanotechnological applications and biological processes.[1-4] Driven by the pursuit of understanding the anomalous phase behavior of confined water, topics such as low-dimensional ice formation,[5-7] unconventional phase transitions,[8-11] and hydrophobic evaporation or dewetting,[12-19] have been extensively studied over the last two decades. The specific manifestation of anomalous water phase behavior depends on the nature of the confining environment, *e.g.* surface chemistries, surface roughness, and/or 1D or 2D geometric boundaries that may or may not be deformable. Graphene, a highly flexible two-dimensional carbon allotrope,[20, 21] has become a paradigmatic example of a 2D hydrophobic confining surface.[22] In graphene nanocapillaries, since the effect of the confining carbon interfaces on water persists at short range (~5 Å),[23, 24] nanoconfined water can adopt a multi-layered structure characterized by strong density fluctuations along the direction of confinement.

Confinement has been shown to play a critical role in the formation of stable multi-layered two dimensional ice,[25-27] which at room temperature forms at pressures on the order of several GPa.[11] Even at ambient pressures the formation of square ice from droplets of water confined between graphene sheets has been observed experimentally,[5] which is possible because the interfacial adhesion forces between the confining graphene surfaces are effectively generating pressures of ~1 GPa within the confined space. Confinement may also give rise to phase coexistence. For example, molecular simulations have revealed a stable liquid water layer that is enveloped between two ice layers under 2D hydrophobic boundaries.[8, 28]

Besides thermodynamic control parameters, such as pressure or temperature, the phase behavior of water under confinement is affected by the commensurability between the confinement distance and the density of water.[5, 8, 11, 27, 28] For example, driven through incommensurate transitions, a transformation from a liquid, to a low-density ice phase, back to a high-density liquid, to finally a high-density ice phase, has been predicted for water nanofilms.[9] In another recent study, it was found that oscillations in the shear viscosity of confined water of several orders of magnitude occur over small variations in the confinement distance (under 1 Å).[29] When the density and confining distance are incommensurate, the system can also exhibit a sharp transition to a different multi-layer state with different types of phases. Giovambattista et al. found a phase transition between a bilayer liquid and a trilayer heterogeneous fluid (THF),

characterized by highly ordered ice layers close to the confining surfaces and a disordered (liquid) middle layer, upon increasing the density of water while keeping the confinement distance constant between 8 - 9 Å.[8] When the confinement distance was kept at 6 Å, a transition between THF and bilayer ice occurred upon decompression instead.

Despite the extensive research efforts, most computational studies have focused on rigid confinement, with only a handful of studies having investigated water confined within flexible surfaces,[5, 12, 30-32] and none have systematically addressed the phase behavior of water under conditions of deformable interfaces. The question we aim to answer here is whether the phase behavior of water mapped under rigid confinement can be extended to the more relevant scenario of flexible confinement, under ambient conditions of temperature and pressure (0.1 MPa and 300 K) that are relevant in most practical applications.

In this paper, we use molecular dynamics simulations at constant ambient pressure and temperature to study the phase behavior of water confined under flexible graphene sheets in which we systematically vary the amount of water in the nanoslit (the 2D density of water, $\rho_{2D}$) and relax the system in the confinement direction so that it reaches an equilibrium confinement distance, $d_{gg}$. We also simulate the same systems using rigid graphene sheets for comparison. We find that both rigid and flexible cases show intervals of $\rho_{2D}$ where the $d_{gg}$ changes systematically from monolayer (ML) to bilayer (BL) to trilayer (TL) commensurate states of the system. However, we find that the phase behavior of water in the different multi-layered states and the transitions between them are qualitatively different for the rigid and flexible cases. Our study provides new comprehensive understanding of the phase behavior of confined water based on a more realistic model of graphene, and we believe it will be useful to interpret experimental results in the future, where graphene is ubiquitously employed.

## RESULTS

**Out-of-Plane Layered Ordering.** We first analyze how the number of layers in the system varies with the 2D density over the range $0.062 < \rho_{2D} < 0.491$, which allows us to sample systems ranging from an incomplete ML to complete TL systems, beyond which most of the system, aside from the water molecules close to the confining surfaces, adopts an equilibrium phase that tends towards bulk conditions. The 2D density, in units of number of water molecules per unit area, is our only control parameter. The confinement distance $d_{gg}$ is not prescribed, but

adopts an equilibrium value for a given $\rho_{2D}$, which differs from the theoretical findings regarding the stability of the water phase which used fixed wall distances.[8, 33] In addition, by using $\rho_{2D}$ as a control parameter, we also avoid making ambiguous assignments of the 3D density under confinement, which requires choosing an ill-defined excluded distance from the confining surfaces.[34]

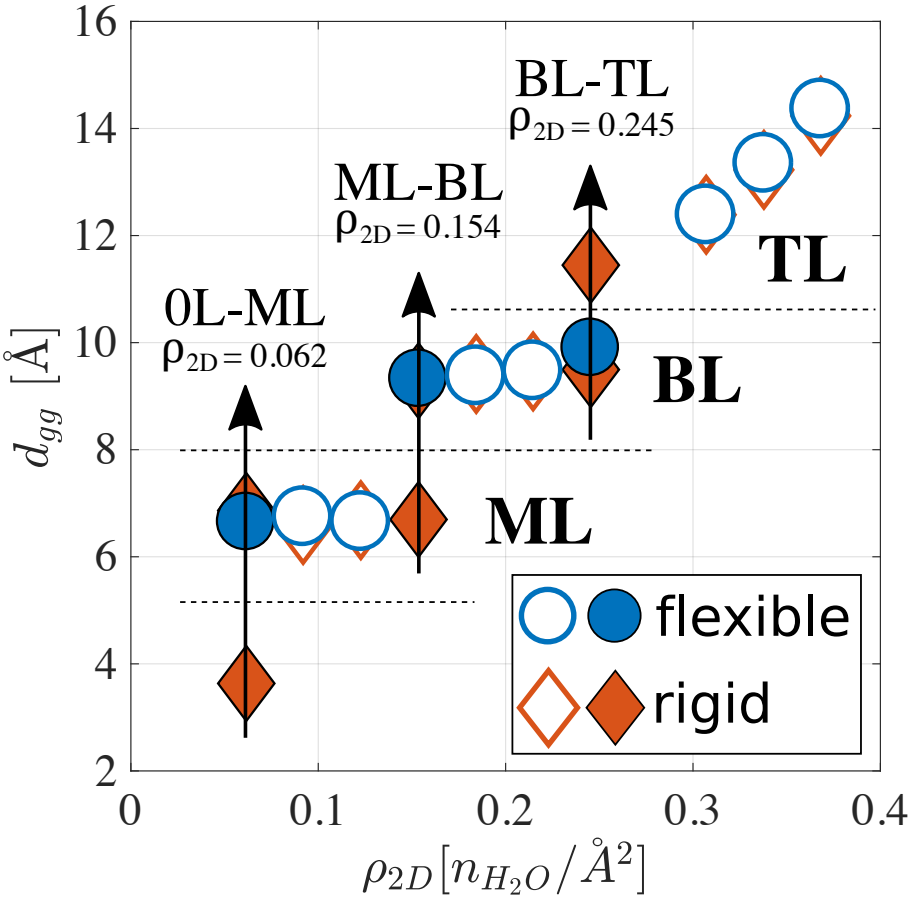


**Figure 1.** *Average confining distance, $d_{gg}$, as a function of the 2D density of water, $\rho_{2D}$.* The average confining distance is calculated by averaging the distance between the graphene sheets at each point in the plane, $d_{gg}(y,z)$, over the whole area, $A = L_y L_z$. The three transitions between no-water to monolayer (0L-ML), monolayer to bilayer (ML-BL), and bilayer to trilayer (BL-TL) are indicated in the plot by full symbols and vertical arrows. The ML, BL, and TL regimes are also illustrated, separated by discontinuous horizontal lines.

Fig. 1 shows the dependence of the equilibrium confining distance on $\rho_{2D}$, for both flexible and rigid cases. We observe three well-defined regimes characterized by small changes of $\langle d_{gg} \rangle$ over relatively large variations in $\rho_{2D}$, which are separated by discontinuous transitions signaled by abrupt changes in $\langle d_{gg} \rangle$ over very small variations in $\rho_{2D}$. The first regime

($\langle d_{gg}\rangle \sim 6-8$ Å and $0.062 < \rho_{2D} < 0.123$) corresponds to ML states, the second regime ($\langle d_{gg}\rangle \sim 8-10$ Å and $0.154 < \rho_{2D} < 0.215$) to BL states, and the third regime ($\langle d_{gg}\rangle > 10$ Å and $\rho_{2D} > 0.245$) corresponds to TL states. In the ML and BL states, the equilibrium confinement distance varies only marginally as $\rho_{2D}$ is increased. For the TL case, however, a linear dependence is observed, $\langle d_{gg}\rangle \propto \rho_{2D}$, which is a signature of bulk behavior since $\rho_{3D} = \rho_{2D}/\langle d_{gg}\rangle$ = constant.[34]

The transitions between the (n)-layer and (n+1)-layer states occur for both rigid and flexible graphene walls at the same values of $\rho_{2D}$, however they are found to be qualitatively different. In the case of rigid walls, the ML-BL and BL-TL transitions are sharp, although more finely spaced density values would be required to quantify whether the two transitions are closer to first or second order behavior. However, for the situation of flexible confinement, we observe a split in the $\langle d_{gg}\rangle$ distances (red filled diamonds in Fig. 1), at the same $\rho_{2D}$ transition values as for the rigid walls. Upon closer inspection into the transition states for the flexible walls, we observe the coexistence of an (n)-layer and an (n+1)-layer state (Figure 2). The heat maps in Fig. 2 show the position the water molecules relative to the graphene sheets as a function of $d_{gg}$ averaged over time. For the lowest density studied, the strong graphene adhesion between the surfaces traps 1D pockets of ice, similar to the phenomena observed in a previous study.[5]

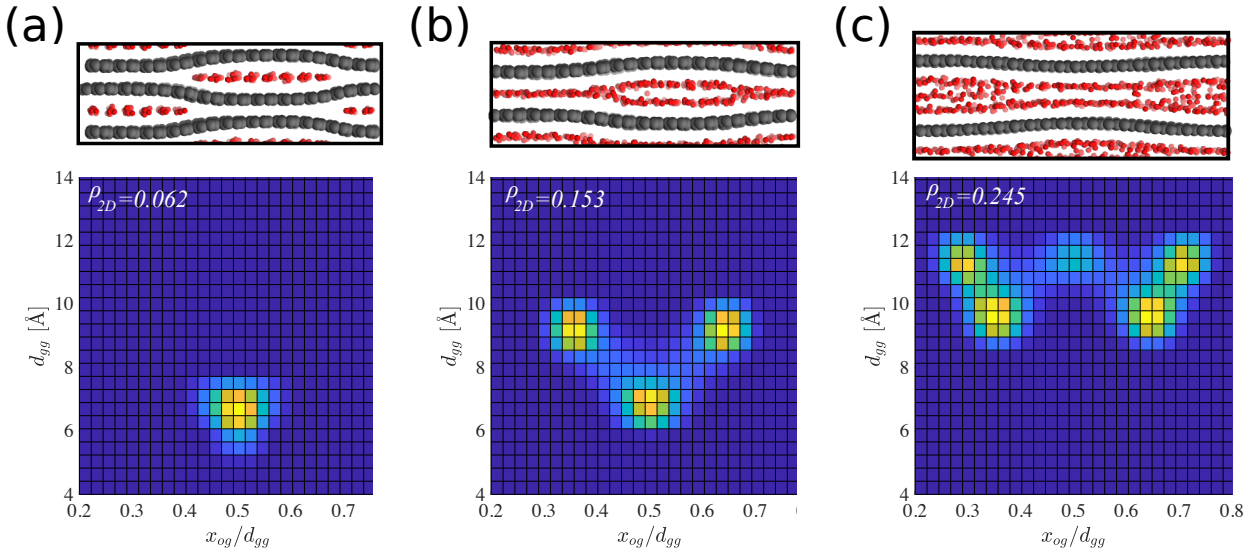


**Figure 2.** *Systems at the transition between multi-layered states for the case of flexible confinement.* (a) 0L-ML, (b) ML-BL, (c) BL-TL. In the snapshots, the oxygen atoms of the water molecules are shown in red, and the carbon atoms of the graphene sheets in grey. In the heat maps on the bottom, warmer colors correspond to a higher probability of finding water there.

The incommensurability of the systems is evidenced by a broadening of the density peaks as illustrated by the BL-TL transition at $\rho_{2D}$= 0.245 (Fig. 3b). At the transition, the probability distributions reveal two broad peaks in the case of rigid confinement and a split to a BL/TL coexisting states in the case of flexible graphene walls. The confining distance for the rigid walls, $d_{gg}$= 9.90 Å, also falls in between the $d_{gg}$ of the BL and TL coexisting states for the flexible walls, which are 9.50 and 11.45 Å, respectively.

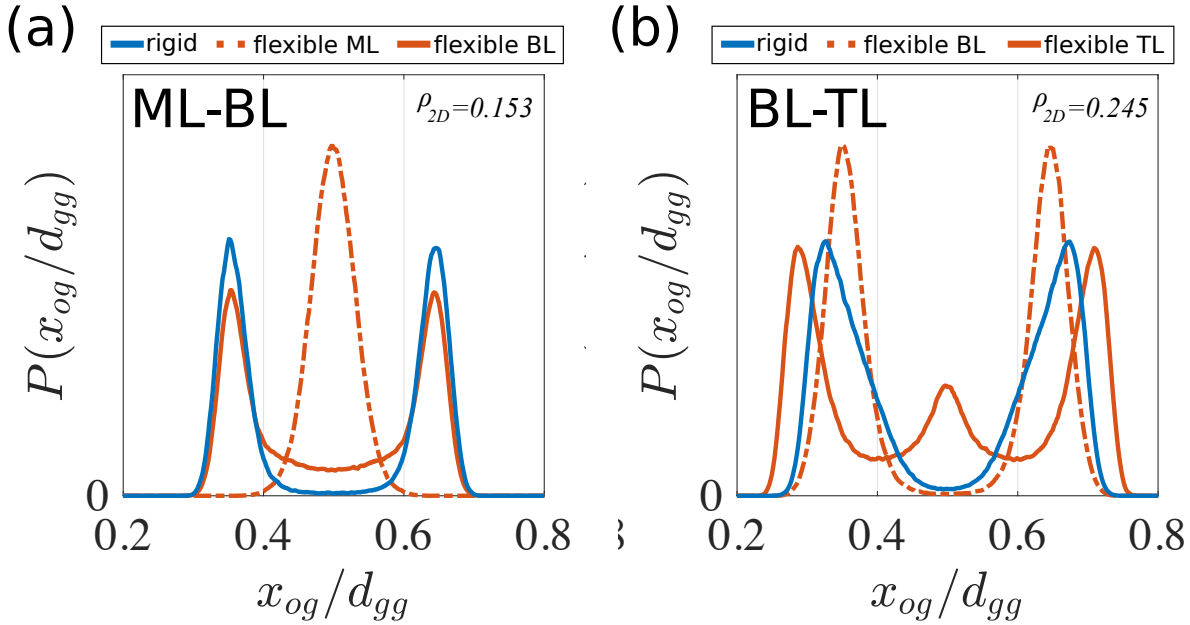


**Figure 3.** *Water density profiles at the transition states for both rigid and flexible walls.* (a) ML-BL transition. (b) BL-TL transition. Because the transition states for the systems with flexible walls correspond to coexisting states of (n)-layer and (n+1)-layer states, those are shown in the plots as dashed and full red lines, respectively.

**In-Plane Structural Order and Dynamics.** Now, we study the structure and dynamics of water to assess the in-plane phase behavior in the commensurate states between the transitions, so that we can discern at a coarse level between ice, liquid, and gas phases. For this purpose, we calculate the oxygen-oxygen pair correlation function $g_{OO}(r)$, the angle distributions between coplanar oxygen nearest neighbors, $p(\theta)$, and the lateral mean-squared-displacement, $D_{//}$, for all the cases (see Methods). We note that the Steinhardt-Nelson order parameters,[35] which are commonly used to identify ice nucleation for 3D ice, were not particularly useful discern among different phases present in the systems studied here.

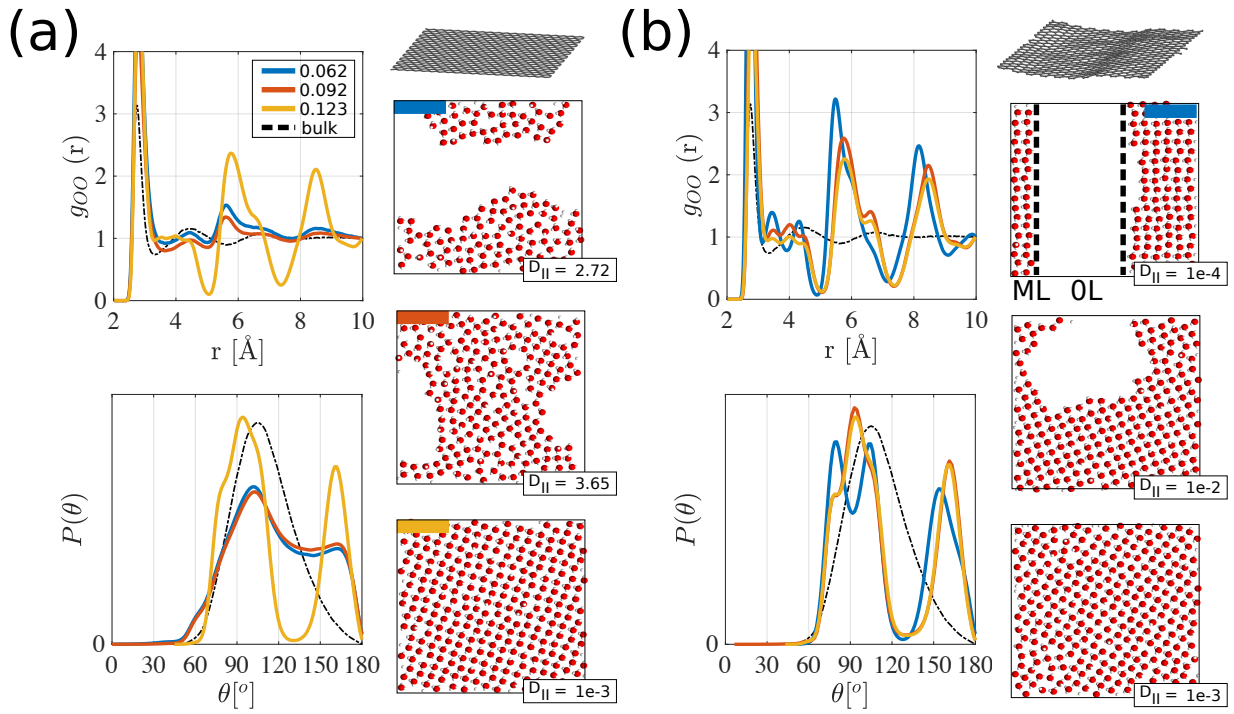


**Figure 4.** *Structure and dynamics of systems in ML regime for $\rho_{2D}$= 0.062 (top), $\rho_{2D}$= 0.092 (middle), $\rho_{2D}$= 0.123 (bottom)*. (a) Rigid walls. (b) Flexible walls. Each panel shows the lateral oxygen-oxygen pair correlation functions, $g_{OO}(r)$, (top), and the angle distributions of coplanar oxygen atoms, $p(\theta)$, (bottom). Snapshots are also shown corresponding to the different cases, and the lateral diffusion coefficients, $D_{||}$, are given in units of $10^{-5}$ cm$^2$/s. The separation between the 0L and the ML ice in the 0L/ML coexisting state is illustrated by a black dashed line in the first snapshot of panel (b).

We start by analyzing the in-plane phase behavior in the ML regime, shown in Fig. 4. For the lowest density investigated, $\rho_{2D}$=0.062, there is not enough water to form a full monolayer. In the case of rigid walls this leads to liquid-vapor coexistence, where the liquid phase is characterized by a diffusivity of $D_{//}$=2.7 x$10^{-5}$ cm$^2$/s (Fig. 4a), similar to the value for bulk water. The ML liquid structure is best described as a highly defective tetrahedral network as seen in the $g_{OO}(r)$ and the broad peak in $p(\theta)$ around the tetrahedral angle $\theta$ =104°.[36] It is worth noting that the peak at $\theta \approx 160^o$ seen in the angular distributions of every case in Figure 4 corresponds to collinear nearest neighbors. By contrast, the flexible graphene system exhibit a rhombic ice structure characterized by peaks in $p(\theta)$ at $\theta$=70°, 110° and 160°, with a diffusivity that is 3-4 orders of magnitude smaller than observed for rigid walls (Fig 4b). The snapshot of the system under flexible confinement reveals a region where there is no water, but unlike the system with

the rigid walls, this area is not a vapor region but a region of graphene-graphene contact (also seen in the snapshot in Figure 2a). When $\rho_{2D} = 0.092$, the rigid graphene walls shows liquid-vapor coexistence, whereas the flexible walls now support the formation of square ice characterized by peak in $p(\theta)$ at $\theta \approx 90^o$. At $\rho_{2D} = 0.123$ there is enough water for a full monolayer, and both the rigid and flexible graphene walls exhibit the formation of square ice, again supported by a structured $g_{OO}(r)$, the peak in $p(\theta)$ at $\theta \approx 90^o$, and the corresponding self-diffusion coefficients with nearly arrested values.

As the water density is increased to $\rho_{2D}$=0.154 the system transitions to the BL regime (Fig. 5). At $\rho_{2D}$=0.154 the system with rigid walls replaces the ice phase with a liquid-vapor coexistence, where the liquid phase has a very similar structure to bulk water as evidenced again by the peak in $p(\theta)$ at $\theta \approx 104^o$ (Fig. 5a). As the water density is increased further to $\rho_{2D}$=0.184 and $\rho_{2D}$=0.245, enough water becomes available to create bilayers with complete liquid coverage. A visual analysis of the trajectories reveals small patches of hexagonal ice that nucleate and dissipate on the time scales of the simulation, suggesting that the systems with rigid walls in the BL regime are close to the solid-liquid phase transition. This is also supported by the substantially slower than bulk self-diffusion coefficient, of the order of $10^{-5}$ cm$^2$/s, observed in all three cases. For the systems with flexible walls (Fig. 5b) we observe at $\rho_{2D}$=0.154 the coexistence of a ML solid and a BL liquid phase, as observed also from simulation snapshot shown in Fig 2b. These coexisting liquid phases are structurally different and the $g_{OO}(r)$ and $p(\theta)$ plots reflect features from both. For example, the position of the 2$^{nd}$ peak in the $g_{OO}(r)$ agrees with the 2$^{nd}$ peak of bulk water and comes from the liquid in the BL region. In the same $g_{OO}(r)$ we also observe significant peaks at ~5.5 Å and ~8.5 Å that reflect the square ice structure of the ML region. The $p(\theta)$ exhibits a broad peak $\theta \approx 100^o$ that includes the peak characteristic of square ice in the ML region ($\theta$ =90°) and that of the tetrahedral network of the liquid in the BL region ($\theta$ =104°). At the higher densities in the BL regime, the flexible system transitions to the liquid state alone. As in the case of rigid confinement the systems are in the cusp of forming hexagonal ice, similarly to that observed for rigid walls. However, the diffusivity in the case of flexible confinement is consistently lower than for rigid confinement. It is also worth noting that the peak in $p(\theta)$ characteristic of collinear neighbors at $\theta \approx 160^o$ is much less significant in the BL than in the ML regime.

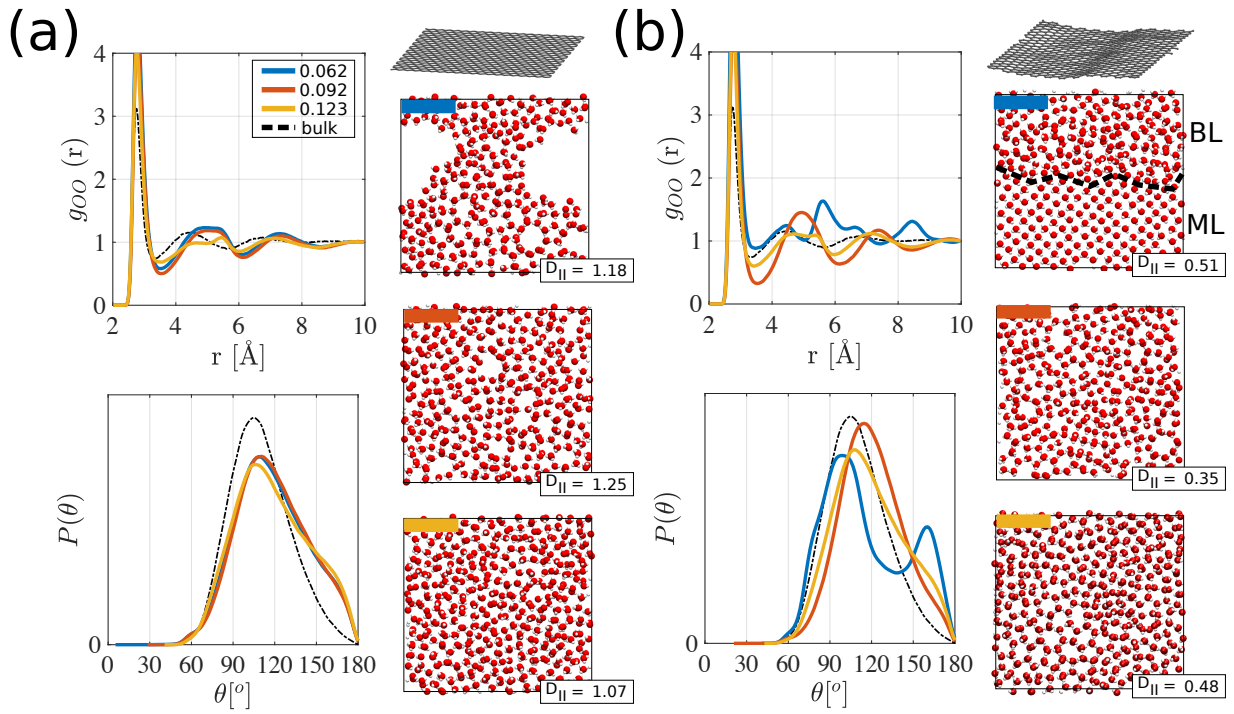


**Figure 5.** *Structure and dynamics, and phase behavior, of systems in BL regime for $\rho_{2D}$= 0.154 (top), $\rho_{2D}$= 0.184 (middle), $\rho_{2D}$= 0.215 (bottom).* (a) Rigid walls. (b) Flexible walls. Each panel shows the lateral oxygen-oxygen pair correlation functions, $g_{OO}(r)$, (top), and the angle distributions of coplanar oxygen atoms, $p(\theta)$, (bottom). Snapshots are also shown corresponding to the different cases, and the lateral diffusion coefficients, $D_{||}$, are given in units of $10^{-5}$ cm$^2$/s. The separation between the regions with ML ice and BL liquid in the ML/BL coexisting state is illustrated by a black dashed line in the first snapshot of panel (b).

When the density is increased beyond $\rho_{2D}$=0.245, the systems transition into the TL state. As the density is increased even further, the intermediate layer of water becomes thicker and more bulk-like, dominating the behavior of the system eventually at larger confining distances, in good agreement with previous studies.[34] In this case we find that the differences between rigid and flexible graphene walls are found to be minor except for slightly higher self-diffusion coefficients in the latter.

## DISCUSSION

In this section we address the real-world applicability of the simulation setup, where the number of confined water molecules is fixed, rather than utilizing some external control parameter such as chemical potential, pressure, or temperature to maintain equilibrium. We performed a small number of simulations where the interlayers were put in contact with a reservoir such that there

is exchange of molecules between the reservoir and the interlayer (Figure 6a). We found the same stable coexisting multilayered states as those found using our original fixed water density setup, supporting the case for coexisting multilayered states of water under flexible confinement.

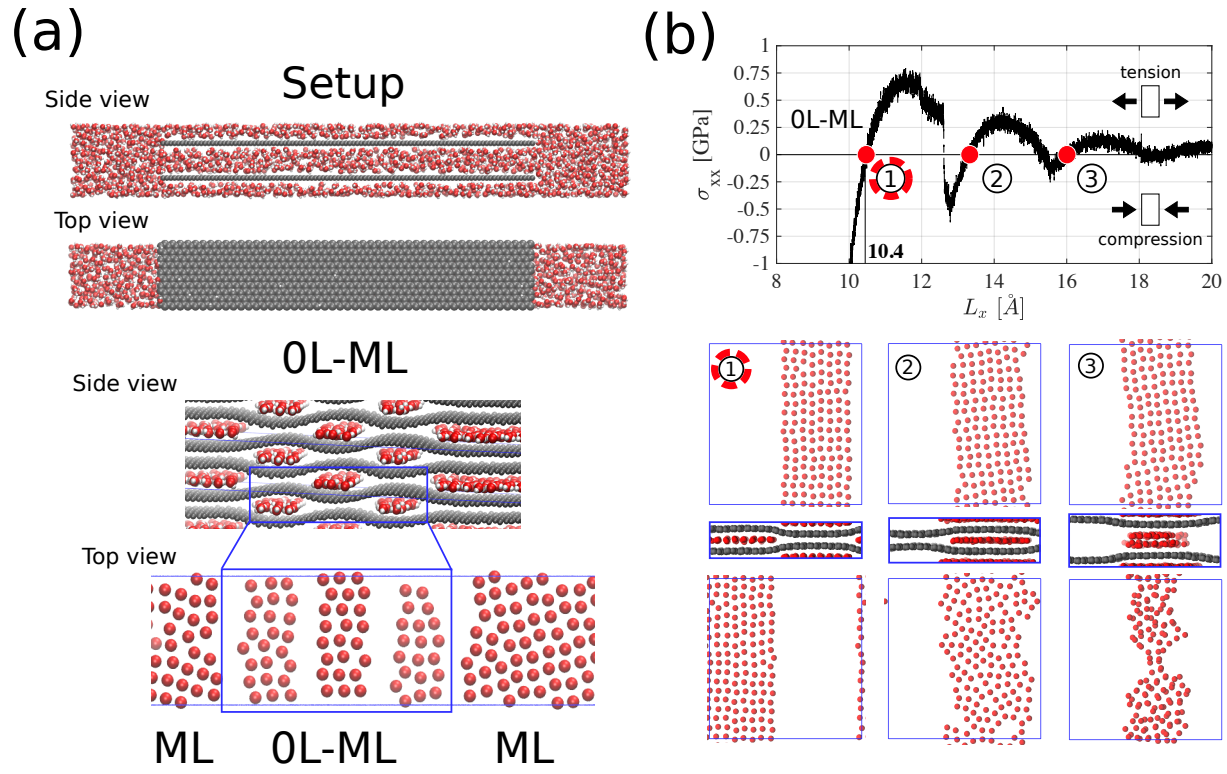


**Figure 6.** *Alternative setups to simulate systems under flexible confinement at the 0L-ML transition*. (a) The graphene confining surfaces are finite in one of the dimensions and the interlayers are in contact with a reservoir. Snapshots of the initial setup are shown above, and side and in-plane views of the equilibrium state below. (b) The setup here is the same as the one used in the rest of the paper but the system is subjected to uniaxial mechanical deformation in the confinement direction. The plot shows the stress response as a function of the simulation box dimensions in the confinement direction, *i.e.* $\sigma_{xx}$ vs. $L_x$. The red circles in the plot indicate local equilibrium states. Snapshots of the side view of the system as well as the plan view of each interlayer for each equilibrium state are shown below the plots. The pressure of water parallel to the confinement direction for the state points is: (1) -0.23 ± 0.18 GPa, (2) 0.07 ± 0.02 GPa, (3) 0.04 ± 0.02 GPa.

Nonetheless, we would contend that simulating systems in equilibrium with an external reservoir is not the most experimentally relevant setup to study the multilayered graphene-based membranes. We find support in the literature that the solvent content and interlayer spacing in the membrane can be adjusted through irreversible kinetically controlled processes. For example,

one such processing technique is “capillary compression” whereby a membrane is first created with a very large solvent content and then is subjected to removal of solvent in a controllable manner by vacuum evaporation. The solvent leaving the system creates capillary forces that decrease the interlayer distance, and once the vacuum evaporation is stopped the system stays with its current solvent content.[37, 38] A different process with similar results is followed by Abraham et al., where the water content in the system is first adjusted by keeping it for very long times at different values of relative humidity, and then it is encapsulated in epoxy so that the water content in the system is preserved.[39] To simulate a typical representative volume element of any one of those experimental systems where the water content is approximately constant but the system is not necessarily in equilibrium with an external reservoir, one needs to study systems like the ones that we present in the paper.

We also evaluate the mechanical stability of the equilibrium states to explore the possibility of other possible metastable states by subjecting the system to uniaxial mechanical perturbations in the confinement direction. We evaluate the stress in the confinement direction, $\sigma_{xx}$, as a function of the simulation box dimension in that direction, $L_x$ for the flexible walls (Fig. 6b) and under rigid confinement (Figure S1-S3). Figure 6b illustrates the existence additional local equilibrium states in the case of flexible confinement at the transition between ML and BL. The maximum stress associated to each subsequent metastable state diminishes from ~0.65 GPa, to ~0.30 GPa, to ~0.15 GPa, suggesting that the first equilibrium state is the most stable. Interestingly, this also holds for all the other systems investigated $\rho_{2D}$= 0.154 (ML-BL) (Fig. S1), and $\rho_{2D}$= 0.245 (BL-TL) (Fig. S2). It is worth noticing that the number of alternative metastable states decreases as we increase $\rho_{2D}$, and also going from flexible to rigid confinement. For example, for $\rho_{2D} = 0.245$ the only mechanically stable equilibrium state is the one shown in Fig. 2 (Fig. S2). This is similar to the conditions employed in other computational studies, *i.e.* fixing the water content in a given system without the system being explicitly in contact with an external reservoir or implicitly via a grand canonical ensemble.[28, 29, 40] In our case, although a variety of metastable states exist for a given $\rho_{2D}$, the coexisting multilayered states we have characterized in this work are the most stable to large mechanical perturbations, which makes them likely to be the most experimentally relevant.

## CONCLUSIONS

In this paper, we have shown that confinement effects in slit nanocapillaries depend strongly on the flexibility of the planar confining surfaces. We find that the transitions between different multi-layered states of nanoconfined water, although occurring at the same density values, are very different between systems with rigid and flexible walls. Remarkably, while the rigid systems exhibit sharp differences in the confinement distances at the transition incommensurate states, the flexible walls allow the system to spatially split into an (n)-layer and an (n+1)-layer coexisting states. This finding suggests that incommensurate states are unfavorable, such that when the constraint of infinite rigidity of the confining surfaces is relaxed, the system splits into two commensurate states with a different number of layers. Although a similar coexisting state has been observed under imposed inhomogeneous confinement,[28] in this study the coexisting states are qualitatively different because we do not impose any inhomogeneity in the system. Furthermore, within the same multi-layer state, the flexible walls introduce a very different sequence of ice phases and phase co-existence with vapor and liquid phases than that observed with rigid walls. The differences can be dramatic. For example, for incomplete monolayers in the ML regime, square and rhombic ice form in the case of flexible walls while water remains liquid for rigid walls. Because flexible interfaces are widely present in both technological and biological processes, it is of critical importance to understand nanoconfinement effects in the phase behavior of water under realistic conditions, beyond the idealized confinement conditions of infinitely rigid walls. This work is a step forward in that direction.

## COMPUTATIONAL METHODS

The model system consists of two parallel graphene sheets with water molecules filling the two interlayers at a prescribed in-plane density $\rho_{2D}$. Periodic boundary conditions are applied in all dimensions and in all dimensions. The confinement direction is *x*, and the in-plane dimensions of the system are $L_y$ = 46.2 Å and $L_z$ = 48.5 Å. We use the TIP4P-Ew model of water,[41] and the parameters for graphene, summarized in Tables S1 and S2, have been adapted from previous work.[14, 42]

All the simulations were performed with the LAMMPS software package[43] found at http://lammps.sandia.gov. We use a time step of 2.0 fs for all the simulations, and all the

simulations are performed at T = 298 K and 1 atm. We use the RATTLE algorithm[44] with a tolerance of $10^{-4}$ to keep the TIP4P-Ew water molecules rigid. We use the particle-particle particle-mesh solver[47] provided in LAMMPS using a relative error in forces of $10^{-4}$ and a cutoff of 9 Å for long-ranged electrostatics.

We equilibrate the systems in two steps. First in order to relieve close contacts or other high-energy configurations in initial system, we run Brownian dynamics[45] for 100 ps using a Langevin thermostat to maintain the temperature at 298 K. During this stage, the displacement of the atoms in a single time step is limited to 0.1 Å. Subsequently, we simulate the system in the NpT ensemble for another 5 ns using a Nose-Hoover extended Lagrangian procedure[46] with a temperature damping parameter of 0.1 ps. A barostat with a damping time of 1 ps is coupled to the confinement dimension $x$ to maintain the pressure at 0.1 MPa. The dimensions of the simulation box are fixed in $y$ and $z$. After equilibration, we run simulations for an additional 10 ns using the same settings. We collect data for analysis every 500 steps (*i.e.* 2 ps). In the rigid cases, the graphene sheets are kept rigid but their center of mass position can fluctuate. In the flexible cases the full force field is employed without further constraints.

**Analysis.** To calculate $g_{OO}(r)$,[36] oxygen atoms within 0.4 Å in the x-direction of the reference atom were considered coplanar. The distances between all coplanar oxygen pairs were then histogrammed:

$$g_{lateral}(r) = \frac{A}{\pi r N^2}\langle \sum_i \sum_{j\neq i} \delta(r - r_{ij})\rangle \quad (1)$$

For the angle distributions $p(\theta)$, $\theta$ is the angle between a central oxygen atom and the first and second nearest neighbors that are within 0.4 Å in the x-direction. We estimate the lateral diffusion coefficient, $D_{||}$, using Einstein's relation, $MSD_{||} = 4\,t\,D_{||}$. The lateral MSD is computed as follows:

$$MSD_{||} = \langle r_{YZ}^2 \rangle = \frac{1}{N}\sum_{i=1}^{N}\left(r_{i,YZ}(t) - r_{i,YZ}(0)\right)^2 \quad (2)$$

**AUTHOR CONTRIBUTIONS:** The manuscript was written through contributions of all authors. All authors have given approval to the final version of the manuscript.

**FUNDING SOURCES:** LRP and THG acknowledge support from the Director, Office of Science, Office of Basic Energy Sciences, Chemical Sciences Division of the U.S. Department of Energy under Contract No. DE-AC02-05CH11231. LF was supported by the National Science Foundation Graduate Research Fellowship under Grant No. DGE 110640.

**ACKNOWLEDGMENTS:** This research used resources of the National Energy Research Scientific Computing Center, a DOE Office of Science User Facility supported by the Office of Science of the U.S. Department of Energy under Contract No. DE-AC02-05CH11231.

**SUPPORTING INFORMATION AVAILABLE:** Force field parameters used in the simulations and additional equilibrium states. This material is available free of charge via the Internet at http://pubs.acs.org

## REFERENCES

[1] Holt, J. K., Park, H. G., Wang, Y., Stadermann, M., Artyukhin, A. B., Grigoropoulos, C. P., Noy, A., and Bakajin, O. (2006) Fast Mass Transport Through Sub-2-Nanometer Carbon Nanotubes, *Science 312*, 1034-1037.

[2] Lucent, D., Vishal, V., and Pande, V. S. (2007) Protein Folding under Confinement: A Role for Solvent, *Proc. Natl. Acad. Sci. USA 104*, 10430-10434.

[3] Levinger, N. E. (2002) Water in Confinement, *Science 298*, 1722-1723.

[4] Nair, R. R., Wu, H. A., Jayaram, P. N., Grigorieva, I. V., and Geim, A. K. (2012) Unimpeded Permeation of Water Through Helium-Leak-Tight Graphene-Based Membranes, *Science 335*, 442-444.

[5] Algara-Siller, G., Lehtinen, O., Wang, F. C., Nair, R. R., Kaiser, U., Wu, H. A., Geim, A. K., and Grigorieva, I. V. (2015) Square Ice in Graphene Nanocapillaries, *Nature 519*, 443-445.

[6] Koga, K., Gao, G. T., Tanaka, H., and Zeng, X. C. (2001) Formation of Ordered Ice Nanotubes Inside Carbon Nanotubes, *Nature 412*, 802-805.

[7] Zhou, W., Yin, K., Wang, C., Zhang, Y., Xu, T., Borisevich, A., Sun, L., Idrobo, J. C., Chisholm, M. F., Pantelides, S. T., Klie, R. F., and Lupini, A. R. (2015) The Observation of Square Ice in Graphene Questioned, *Nature 528*, E1-E2.

[8] Giovambattista, N., Rossky, P. J., and Debenedetti, P. G. (2009) Phase Transitions Induced by Nanoconfinement in Liquid Water, *Phys. Rev. Lett. 102*, 050603.

[9] Han, S., Choi, M. Y., Kumar, P., and Stanley, H. E. (2010) Phase Transitions in Confined Water Nanofilms, *Nat. Phys. 6*, 685-689.

[10] Mochizuki, K., and Koga, K. (2015) Solid-Liquid Critical Behavior of Water in Nanopores, *Proc. Natl. Acad. Sci. 112*, 8221-8226.

[11] Zhu, Y., Wang, F., Bai, J., Zeng, X. C., and Wu, H. (2015) Compression Limit of Two-Dimensional Water Constrained in Graphene Nanocapillaries, *ACS Nano 9*, 12197-12204.

[12] Altabet, Y. E., Haji-Akbari, A., and Debenedetti, P. G. (2017) Effect of Material Flexibility on The Thermodynamics and Kinetics of Hydrophobically Induced Evaporation of Water, *Proc. Natl. Acad. Sci.114*, E2548-E2555.
[13] Head-Gordon, T., and Lynden-Bell, R. M. (2008) Hydrophobic Solvation of Gay-Berne Particles in Modified Water Models, *J. Chem. Phys. 128*, 104506.
[14] Hummer, G., Rasaiah, J. C., and Noworyta, J. P. (2001) Water Conduction Through the Hydrophobic Channel of a Carbon Nanotube, *Nature 414*, 188-190.
[15] Sharma, S., and Debenedetti, P. G. (2012) Evaporation Rate of Water in Hydrophobic Confinement, *Proc. Natl. Acad. Sci. 109*, 4365-4370.
[16] Chandler, D. (2002) Hydrophobicity: Two Faces Of Water, *Nature 417*, 491-491.
[17] Choudhury, N., and Pettitt, B. M. (2007) The Dewetting Transition and the Hydrophobic Effect, *J. Amer. Chem. Soc. 129*, 4847-4852.
[18] Eslami, H., and Heydari, N. (2014) Hydrogen Bonding in Water Nanoconfined Between Graphene Surfaces: A Molecular Dynamics Simulation Study, *J. Nanopart. Res. 16*, 2154-2158.
[19] Eslami, H., Mozaffari, F., Moghadasi, J., and Müller-Plathe, F. (2008) Molecular Dynamics Simulation of Confined Fluids in Isosurface-Isothermal-Isobaric Ensemble, *J. Chem. Phys. 129*, 194702.
[20] Wei, Y., Wang, B., Wu, J., Yang, R., and Dunn, M. L. (2013) Bending Rigidity and Gaussian Bending Stiffness of Single-Layered Graphene, *Nano Lett. 13*, 26-30.
[21] Fasolino, A., Los, J. H., and Katsnelson, M. I. (2007) Intrinsic Ripples in Graphene, *Nat. Mater. 6*, 858--861.
[22] Geim, A. K., and Novoselov, K. S. (2007) The Rise of Graphene, *Nat. Mater. 6*, 183-191.
[23] Chialvo, A. A., and Vlcek, L. (2016) Can We Describe Graphene Confined Water Structures as Overlapping of Approaching Graphene-Water Interfacial Structures? *J. Phys. Chem. C 120*, 7553-7561.
[24] Cicero, G., Grossman, J. C., Schwegler, E., Gygi, F., and Galli, G. (2008) Water Confined in Nanotubes and between Graphene Sheets: A First Principle Study, *J. Amer. Chem. Soc. 130*, 1871-1878.
[25] Chen, J., Schusteritsch, G., Pickard, C. J., Salzmann, C. G., and Michaelides, A. (2017) Double-Layer Ice From First Principles, *Phys. Rev. B 95*, 094121.
[26] Corsetti, F., Matthews, P., and Artacho, E. (2016) Structural and Configurational Properties of Nanoconfined Monolayer Ice from First Principles, *Sci. Rep. 6*, 18651.
[27] Satarifard, V., Mousaei, M., Hadadi, F., Dix, J., Sobrino Fernandez, M., Carbone, P., Beheshtian, J., Peeters, F. M., and Neek-Amal, M. (2017) Reversible Structural Transition in Nanoconfined Ice, *Phys. Rev. B 95*, 064105.
[28] Qiu, H., Zeng, X. C., and Guo, W. (2015) Water in Inhomogeneous Nanoconfinement: Coexistence of Multilayered Liquid and Transition to Ice Nanoribbons, *ACS Nano 9*, 9877-9884.
[29] Neek-Amal, M., Peeters, F. M., Grigorieva, I. V., and Geim, A. K. (2016) Commensurability Effects in Viscosity of Nanoconfined Water, *ACS Nano 10*, 3685-3692.
[30] Deshmukh, S. A., Kamath, G., and Sankaranarayanan, S. K. R. S. (2014) Comparison of the Interfacial Dynamics of Water Sandwiched Between Static and Free-Standing Fully Flexible Graphene Sheets, *Soft Matter 10*, 4067-4083.

[31] Lin, H., Schilo, A., Kamoka, A. R., Severin, N., Sokolov, I. M., and Rabe, J. P. (2017) Insight Into The Wetting of a Graphene-Mica Slit Pore with a Monolayer of Water, *Phys. Rev. B 95*, 195414.
[32] Günther, G., Prass, J., Paris, O., and Schoen, M. (2008) Novel Insights into Nanopore Deformation Caused by Capillary Condensation, *Phys. Rev. Lett. 101*, 086104.
[33] Kumar, P., and Han, S. (2012) Dynamics of Two-Dimensional Monolayer Water Confined in Hydrophobic and Charged Environments, *J. Chem. Phys. 137*, 114510.
[34] Hamid, M., Saman, A., Kowsari, M. H., and Bijan, N. (2012) Simulations of Structural and Dynamic Anisotropy in Nano-Confined Water between Parallel Graphite Plates, *J. Chem. Phys. 137*, 184703.
[35] Steinhardt, P. J., Nelson, D. R., and Ronchetti, M. (1981) Icosahedral Bond Orientational Order in Supercooled Liquids, *Phys. Rev. Lett. 47*, 1297-1300.
[36] Stillinger, F. H., and Head-Gordon, T. (1993) Perturbational View of Inherent Structures in Water, *Phys. Rev. E 47*, 2484-2490.
[37] Cheng, C., Jiang, G., Garvey, C. J., Wang, Y., Simon, G. P., Liu, J. Z., and Li, D. (2016) Ion Transport in Complex Layered Graphene-Based Membranes with Tuneable Interlayer Spacing, *Sci. Adv. 2*.
[38] Yang, X., Cheng, C., Wang, Y., Qiu, L., and Li, D. (2013) Liquid-Mediated Dense Integration of Graphene Materials for Compact Capacitive Energy Storage, *Science 341*, 534.
[39] Abraham, J., Vasu, K. S., Williams, C. D., Gopinadhan, K., Su, Y., Cherian, C. T., Dix, J., Prestat, E., Haigh, S. J., Grigorieva, I. V., Carbone, P., Geim, A. K., and Nair, R. R. (2017) Tunable Sieving of Ions using Graphene Oxide Membranes, *Nat. Nanotechnol.12*, 546.
[40] Compton, O. C., Cranford, S. W., Putz, K. W., An, Z., Brinson, L. C., Buehler, M. J., and Nguyen, S. T. (2012) Tuning the Mechanical Properties of Graphene Oxide Paper and Its Associated Polymer Nanocomposites by Controlling Cooperative Intersheet Hydrogen Bonding, *ACS Nano 6*, 2008-2019.
[41] Horn, H. W., Swope, W. C., Pitera, J. W., Madura, J. D., Dick, T. J., Hura, G. L., and Head-Gordon, T. (2004) Development of an Improved Four-Site Water Model for Biomolecular Simulations: TIP4P-Ew, *J. Chem. Phys. 120*, 9665-9678.
[42] Patra, N., Wang, B., and Kral, P. (2009) Nanodroplet Activated and Guided Folding of Graphene Nanostructures, *Nano Lett. 9*, 3766-3771.
[43] Plimpton, S. (1995) Fast Parallel Algorithms for Short-Range Molecular-Dynamics, *J. Comp. Phys. 117*, 1-19.
[44] Andersen, H. C. (1983) Rattle - a Velocity Version of the Shake Algorithm for Molecular-Dynamics Calculations, *J. Comp. Phys. 52*, 24-34.
[45] Schneider, T., and Stoll, E. (1978) Molecular-Dynamics Study of a Three-Dimensional One-Component Model for Distortive Phase Transitions, *Phys. Rev. B 17*, 1302--1322.
[46] Martyna, G. J., Tobias, D. J., and Klein, M. L. (1994) Constant-Pressure Molecular-Dynamics Algorithms, *J. Chem. Phys.101*, 4177-4189.
[47] Hockney, R. W., and Eastwood, J. W. (1989) *Computer Simulation using Particles*, Hilger, Bristol.

**TOC FIGURE**

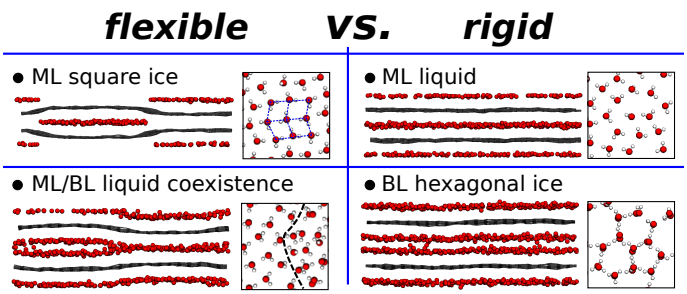
flexible vs. rigid
• ML square ice
• ML liquid
• ML/BL liquid coexistence
• BL hexagonal ice